applied sciences

MDPI

Article

Observation and Numerical Simulation of a Windshear Case at an Airport in the Qinghai-Tibet Plateau

Pak Wai Chan [1,*], Kai Kwong Lai [1], Jiafeng Zheng [2], Yu Zhang [2], Haoming Chen [3] and Xiaoming Shi [3]

[1] Hong Kong Observatory, Hong Kong, China
[2] Plateau Atmosphere and Environment Key Laboratory of Sichuan Province, School of Atmospheric Sciences, Chengdu University of Information Technology, Chengdu 610225, China
[3] Division of Environment and Sustainability, Hong Kong University of Science and Technology, Hong Kong, China
* Correspondence: pwchan@hko.gov.hk

Abstract: This paper documents a windshear case for an airport in the Qinghai-Tibet Plateau and explores, for the first time, the capability for high-resolution numerical weather simulation of the wind shear features. The windshear appears to be associated with pulses of the wind speed in a low-level easterly jet. The features are basically reproduced quite well with the high-resolution numerical model, though some discrepancies are identified, such as the maximum wind speed of the easterly jet and the magnitude of the eddy dissipation rate as compared with the actual Doppler LIDAR observations. Statistical analysis has been performed between the observation and the simulation results. The sensitivity of the modeling result to the choice of turbulence parameterization scheme has also been studied. The study result shows that it is possible to forecast the windshear feature using a high-resolution numerical weather prediction model for an airport in the complex terrain of the Plateau.

Keywords: windshear; observation numerical simulation; airport; Qinghai-Tibe Plateau

Citation: Chan, P.W.; Lai, K.K.; Zheng, J.; Zhang, Y.; Chen, H.; Shi, X. Observation and Numerical Simulation of a Windshear Case at an Airport in the Qinghai-Tibet Plateau. *Appl. Sci.* **2024**, *14*, 10981. https://doi.org/10.3390/app142310981

Academic Editor: Dimitris Kaskaoutis

Received: 30 August 2024
Revised: 23 November 2024
Accepted: 24 November 2024
Published: 26 November 2024

1. Introduction

An airport located in an area of complex terrain may be susceptible to the low-level windshear and turbulence due to terrain disruption of the airflow in favorable meteorological conditions (Boilley and Mahfouf (2013) [1], Hon and Chan (2022) [2]). The Hong Kong International Airport is an example of a busy airport located near mountainous terrain. Significant windshear occurs at a rate of about once in every 500 movements. Real-time alerting of windshear and turbulence, particularly for clear air situations for terrain-disrupted airflow, is now made possible with the advancement of remote-sensing meteorological instruments such as the more common usage of Doppler Light Detection And Ranging (LIDAR) systems (Shun and Chan, 2008) [3]. At the same time, short-term forecasting of low-level windshear has also been explored. In a recent study (Chan et al., 2021) [4], a numerical modeling system with a horizontal resolution of 40 m is found to show positive skills in capturing low-level windshear using pilot reports of windshear as the sky truth.

Significant windshear refers to a change in headwind of 15 knots or more, over a distance of several hundreds of meters up to several kilometers, resulting from changes in wind speed and/or wind direction. It may cause the aircraft to deviate from its intended flight path. Significant windshear near the ground could be hazardous because of the limited space left from the ground for the maneuvering of the aircraft. Timely alerting of windshear, by detection and/or by forecasting by numerical weather prediction models, would be crucial in the assurance of aviation safety.

In China, there are a number of airports located in the mountainous area of the Qinghai-Tibet Plateau. Windshear and turbulence have often been reported at the airports in this region (Lin et al., 2021) [5]. In the international meteorological and air traffic journals, there

is rather limited documentation of windshear and turbulence for airports in the Plateau, especially the mechanism of windshear. To the knowledge of the authors, there does not seem to be high-resolution numerical simulation of the terrain-disrupted airflow in aviation applications for this region as well, though there are studies about high-resolution numerical simulations for other airports (e.g., [6–8]). The applicability of the method, e.g., as described in Chan et al. (2021) [4] for the airports in that region, would be an interesting topic scientifically with practical application values. Moreover, in the previous results reported in the literature, the airport is close to isolated high-rising terrain only. For the Qinghai-Tibet Plateau, it consists of very extensive terrain with highly varying heights. It would be interesting to study the terrain-induced windshear over there, to explore the usefulness of high-resolution numerical weather prediction models in forecasting abrupt wind changes.

Large eddy simulation (LES) studies for meteorological applications have been considered in a number of studies in the literature. Ito (2020) [9] and Shimoyama (2013) [10] have considered applications for LES for a couple of airports in Japan. Krishnamurthy et al. (2010) [11] have considered the LES simulation of the eddy dissipation rate (EDR), which is an internationally adopted metric for turbulence, for a complex terrain for T-REX experiment in the US. The verification of LES has also been conducted for a long period of time in a relatively flat area in the Netherlands (Schalkwijk et al., 2015) [12].

This short letter documents a case of windshear at an airport at the Plateau. For the first time, a high spatial resolution (40 m) numerical weather prediction model is used to explore the feasibility of reproducing the main features of the wind that may be related to the windshear. A key element in the simulation of the wind at high spatial resolution is the choice of turbulence parameterization scheme, as discussed in Chan et al. (2022) [13]. Two sets of turbulence parameterization have been tried out with the numerical model, and the results are compared with the actual observations to see which choice appears to be better. One objective of the present study is to find out which turbulence parameterization scheme available in RAMS gives better results in comparison with the actual observations.

2. Materials and Methods

2.1. Equipment in Use

The airport in question is located in the eastern part of the Plateau. Some background information about this airport can be found in Huang et al. (2022) [14]. The terrain near the airport is shown in Figure 1a. The layout of the runway and the instruments are given in Figure 1b. One important piece of instrument for wind observation is the Doppler Wind LIDAR (DWL) manufactured in Shanghai, China. The location is shown in Figure 1b, and a picture of the instrument is given in Figure 1c.

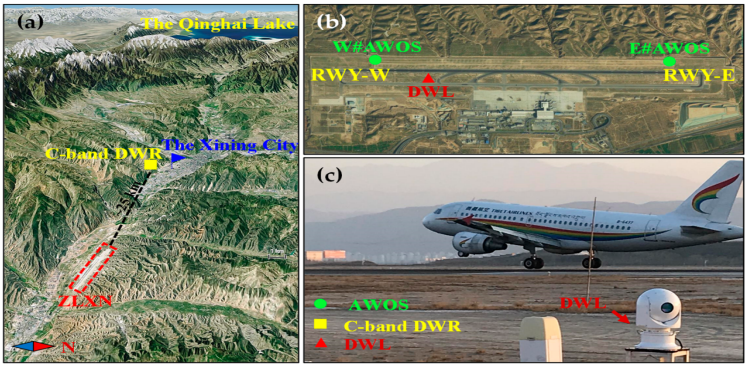

Figure 1. The terrain near the airport (**a**), the runway of the airport (**b**), and the instrument at the airport (**c**). AWOS is the automatic weather observing system, and DWR is the Doppler Weather Radar using a microwave beam. RWY means runway. The red dashed line area is the runway area, and the black dash line is the line of sight of the radar with respect to the runway orientation. The figure has been adopted from [14].

2.2. The Wind and EDR Observations

The DWL provides continuous measurements of the vertical wind profiles. The major wind features of interest in the present study are shown in Figure 2. The period under consideration is 30 November to 1 December 2017. Of particular importance is the occurrence of a low level easterly jet (Figure 2a), reaching 50 knots at the core of the jet. There is veering of the wind with height. In the early morning of 1 December 2017, the low level winds changed to westerly gradually, and the vertical extent of the westerly winds increased gradually with height.

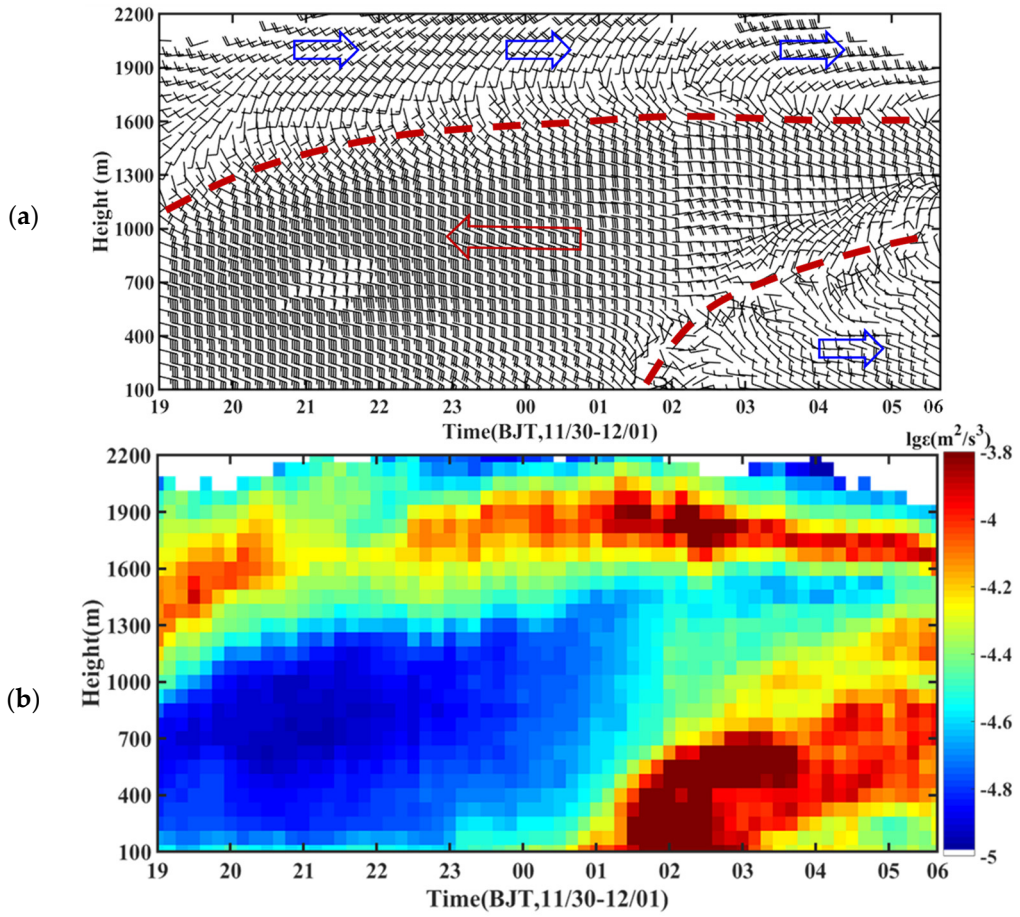

Figure 2. The time–height cross-section of the wind ((**a**), upper panel) and EDR ((**b**), lower panel) as obtained by the DWL for this windshear case. The circle in (**a**) is the area of higher wind speed, with the arrows showing the general wind direction and the broken lines showing the locations of the rapid changes in the wind direction. To better distinguish between the easterly and the westerly winds, the former is shown with a red arrow and the latter is shown with blue arrows. Time is in Beijing Time (BJT), which is 8 h ahead of UTC. In both (**a**) and (**b**), the height refers to the height above ground level.

Using the DWL data, the eddy dissipation rate (EDR), a metric of turbulence for aviation application, has been calculated using the formula below (Bouniol et al., 2004) [15]:

$$EDR = 2\pi\left(\frac{2}{3a}\right)^{3/2}\frac{\sigma_v^3}{\left(L^{2/3}-L_1^{2/3}\right)^{3/2}}$$

where a is the universal Kolmogorov constant with a value of 1.62; σ_v is the spectrum width of Doppler velocities within the sampling time t; L represents the length of larger eddies

passing through the DWL beams within a time interval t, and can be given as $L \approx V_H t$, V_H is the horizontal wind speed; and L_1 is the horizontal length of the DWL sampling volume.

The resulting time–height cross section of the EDR is shown in Figure 2b. Higher turbulence is detected at two regions: first, at heights above the jet core with the veering of the wind, and second, the interface between the easterly wind and the intrusion of westerly wind.

By taking a closer look at the easterly jet, it is found that the wind speed is not uniform with time but there are pulses of higher wind speed, as shown in Figure 3a. The time series of the wind speed at the jet core as well as above and below the jet are shown in Figure 3b. Three pulses of the wind have been identified and highlighted in Figure 3b. This pulsation is believed to give rise to the windshear that may be encountered by the aircraft at the airport.

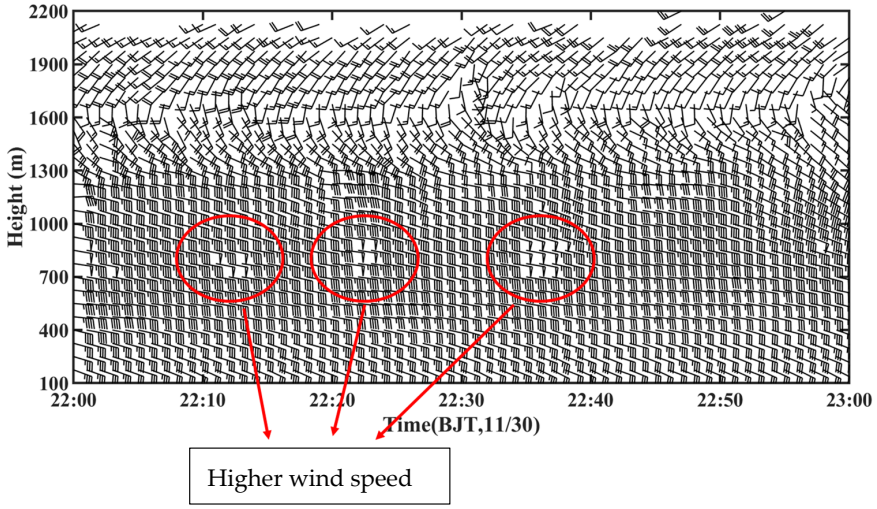

(**a**)

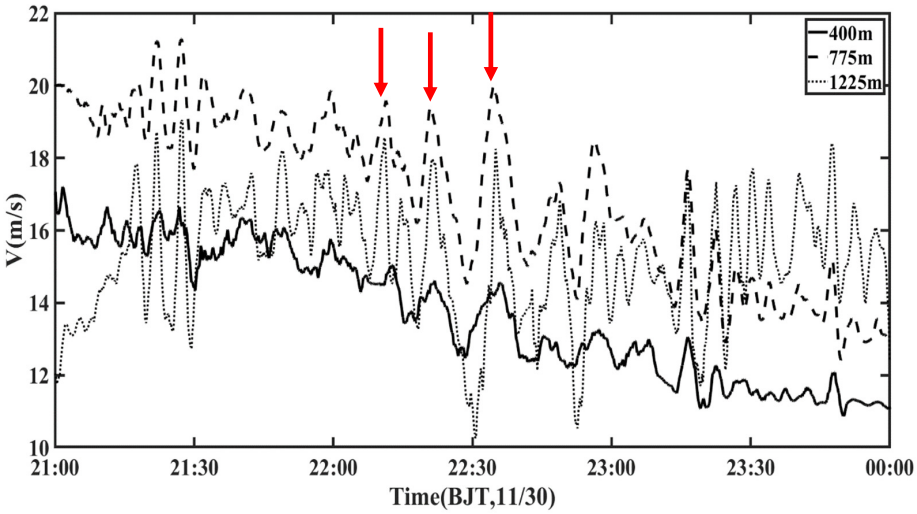

(**b**)

Figure 3. A closer look at the time–height cross-section of the wind (**a**) from DWL with the height to be above ground level, and the time series of the wind at the jet core as well as around the jet (**b**). The instances with higher wind speeds are highlighted in arrows in (**b**).

2.3. The Research Method: Setup of the Numerical Model and Calculation of EDR

The objective of the numerical simulation is to study the feasibility of reproducing the main features of the wind in this windshear case, namely, the easterly jet, the intrusion of

westerly wind, the EDR distribution with time and height, and the wind speed of the jet core and the pulsation of the wind speeds in the jet. Apart from the changes in the synoptic weather pattern, such features are believed to be closely associated with the complex terrain in the region. In order to capture the terrain features, a numerical weather prediction model, namely, the Regional Atmospheric Modeling System (RAMS) version 6.3 with a high horizontal resolution (40 m), has been adopted for the simulation. The setup of the model is similar to that reported by Chan et al. (2021) [4].

The terrain considered in the simulation is shown in Figure 4. As in the previous study, five nested domains have been used. The outermost domain uses the reanalysis data from the National Centers for Environmental Prediction. It is nested downward and the innermost domain (G5) is shown in Figure 4c around the airport area. The physical schemes used in the model are the same as those in Chan et al. (2021) [4].

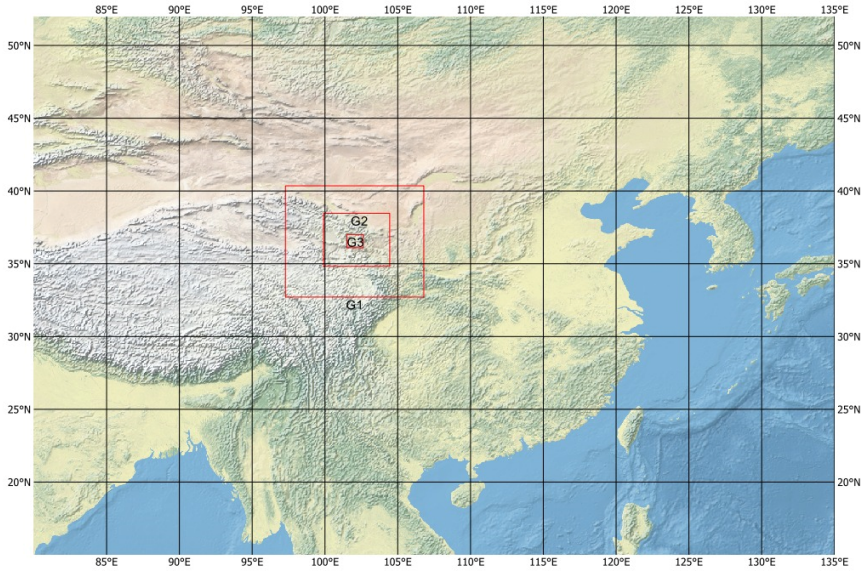

(**a**) Domains G1 to G3

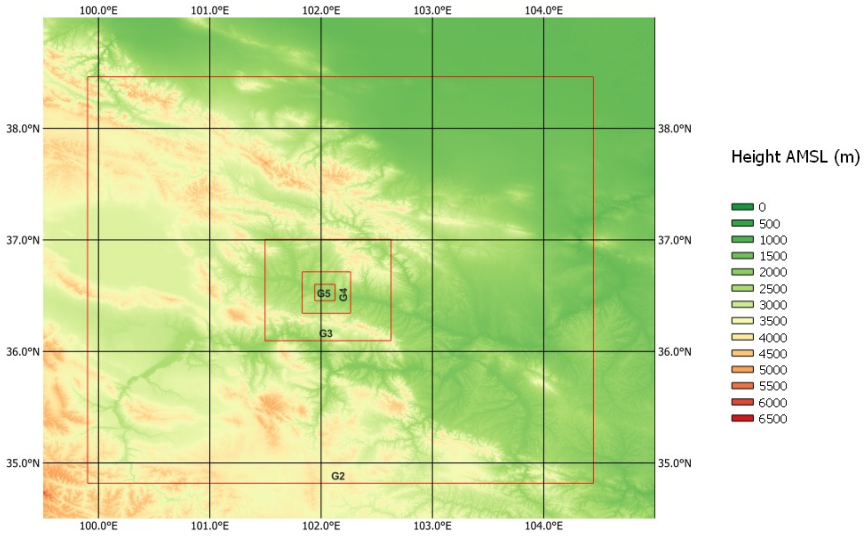

(**b**) Domains G2 to G5

Figure 4. *Cont.*

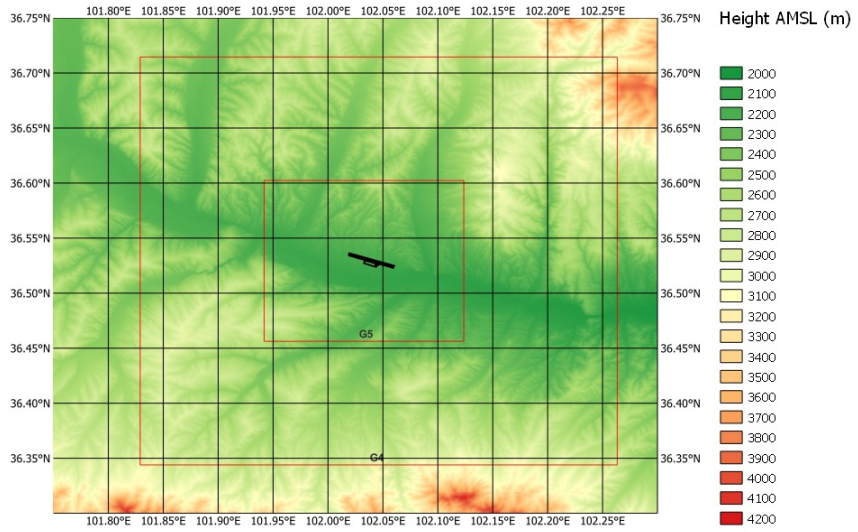

(**c**) a zoom-in of Domains G4 and G5

Figure 4. The five nested domains G1 to G5.

For the turbulence parameterization scheme, as the first attempt, the Smagorinsky (1963) [16] scheme was used in the first two nested domains, and the Deardorff (1980) [17] scheme is used in the last three domains. The sensitivity to the choice of turbulence parameterization scheme would be discussed later.

The wind field data from numerical simulations with a rectangular grid can be utilized to calculate EDR by using the explicit filtering and reconstruction in turbulence parameterization (Chow et al., 2005) [18]. In this method, Subfilter scales can be divided into resolvable subfilter scales (RSFS) and subgrid scales (SGS). We only calculated RSFS part since it accounts for most of the energy. We did zero-order reconstruction in this study so we have $\widetilde{\overline{u}_i^*} = \widetilde{\overline{u}_i}$. Here, the overline represents the filter, the tilde represents discretization, and $\widetilde{\overline{u}_i}$ is the variable from the model.

The RSFS turbulent kinetic energy (TKE) is calculated by

$$\mathrm{TKE} = \frac{1}{2}\left(\widetilde{\overline{u}_i^*}\,\widetilde{\overline{u}_i^*} - \widetilde{\overline{u}_i}^*\,\widetilde{\overline{u}_i}^*\right)$$

Assuming the scale of turbulence is included in inertial subrange, the EDR can be expressed as follows:

$$\varepsilon^{1/3} = \left(\mathrm{TKE}^{3/2}/L\right)^{1/3}$$

Here, we used Butterworth filter horizontally and 1-2-1 filter (Chow et al., 2005) [18] vertically. $L = (\lambda \Delta x \Delta y \Delta z)^{1/3}$ is the scale of the turbulence, Δx, Δy and Δz are grid spacings, and the λ can be derived based on the cutoff wavelength of the filter.

Basically, the same simulation setup as in Chan et al. (2021) [4] is adopted here. But this is the first time that this simulation setup is applied outside Hong Kong, especially in an area of complex terrain as in the Plateau. Moreover, the new formulation of the calculation of EDR is adopted for this model setup for the first time. These are the novel features of the present paper.

3. Results and Discussion

3.1. Simulation Result

The time–height cross section of the simulated wind and EDR at the location of the DWL is shown in Figure 5a. There are a number of findings:

(a) The easterly jet is reproduced in the simulation, though the maximum wind speed at the jet core is less than actual (only around 35 knots of wind speed has been simulated). There is a veering of the wind above the jet;

(b) The intrusion of the westerly jet is also reproduced well, though it occurs later than the actual observation by about 8 h (i.e., 02 local time in actual observations, but around 10 local time in numerical simulation). Moreover, the speed at which the vertical extent of the westerly increases with time is less than actual. The vertical extension of the westerly jet is also lower than actual. By close examination of the data, it is found that these features may be related to the limitation of the global model analysis in this area of complex terrain, as well as the limitation of the amount of data in the Plateau region for more accurate analysis of the wind field, especially in the atmospheric boundary layer;

(c) The main features of the EDR distribution is generally reproduced, namely, higher EDR above the jet at the veering of the wind, and the interface between the easterly and the westerly. However, the EDR values appear to be larger than actual observations.

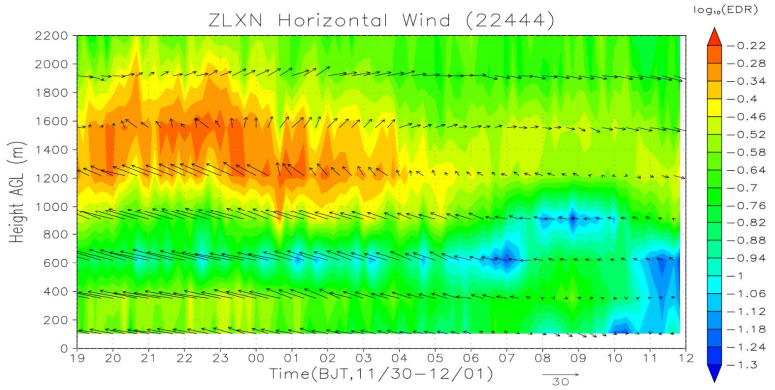

(**a**)

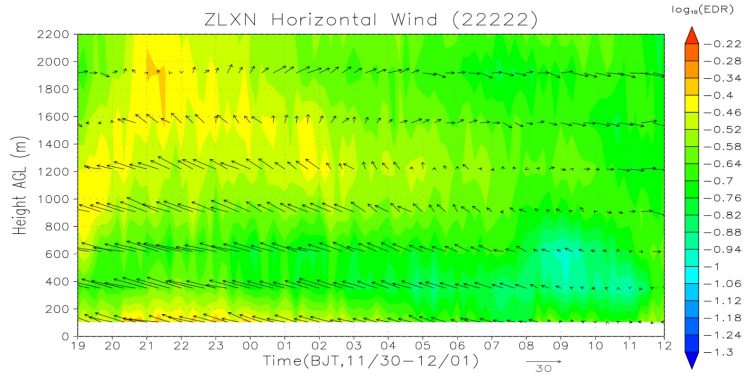

(**b**)

Figure 5. (**a**) is the simulation result of Deardorff scheme, showing the time–height cross section of the simulated wind and EDR. (**b**) is the simulation result of the Smagorinsky scheme.

Another feature of the time–height cross section is the descending of the westerly jet at around 1200 to 1500 m. This is related to the change in the flow regime in the mid-tropospheric westerly in the Plateau region. This is important for en-route stage of the aircraft but is not related to the discussion of windshear, which is the main focus of the present study.

For better visualization of the airflow, the simulated surface wind (with a height of 10 m above ground level) pattern at the innermost domain is shown in Figure 6. In general, the model simulation shows the weaker easterly wind at first, the setting in of the

easterly jet, the prevailing of stronger easterly winds, and the retreat of the easterly with the replacement by the westerly. Though there are no actual observations in the region to confirm the reliability of the simulated airflow, the changes in the wind appear to be reasonable as compared with the limited observations available from the DWL.

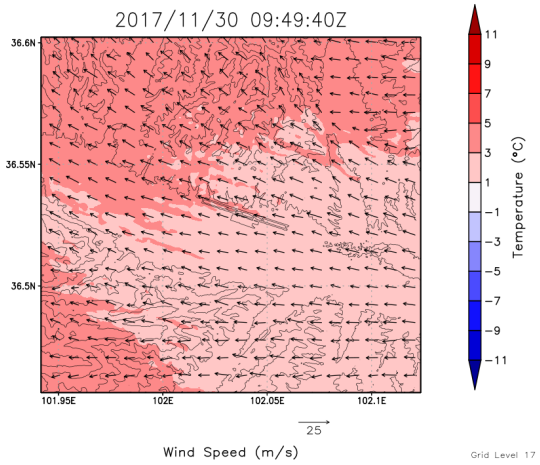

(**a**)

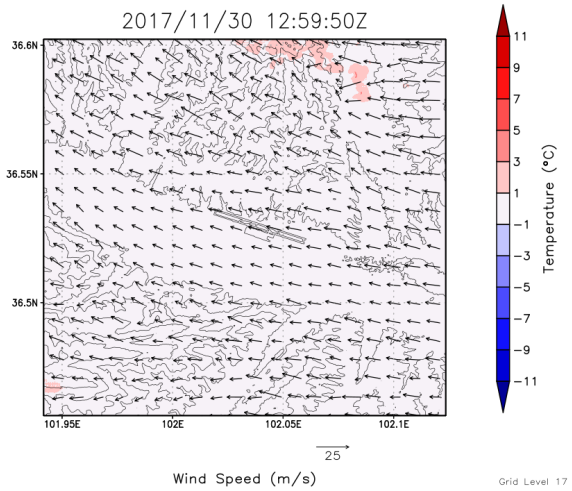

(**b**)

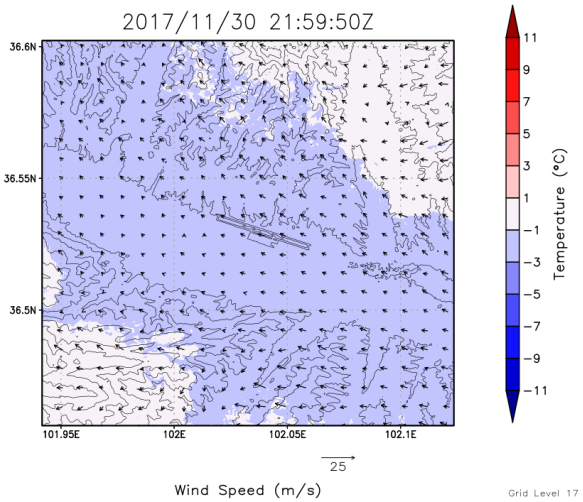

(**c**)

Figure 6. *Cont.*

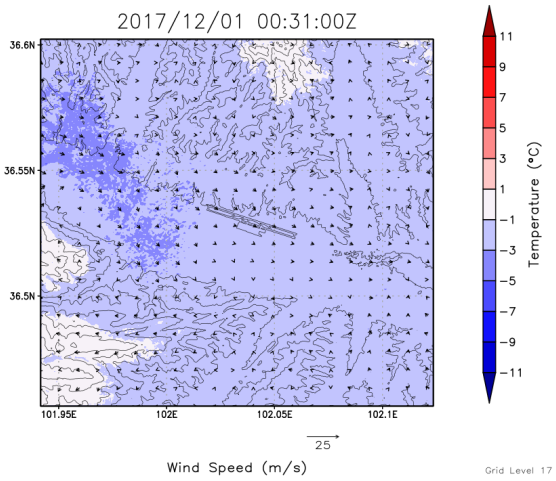

(**d**)

Figure 6. The simulated surface wind patterns at four time instances of the simulation. The times of the plots are shown at the top of each sub-figure (**a**–**d**).

Similar to Figure 3b, the time series of the simulated wind speed at the jet core as well above and below the jet is shown in Figure 7a. The simulation appears to reasonably well reproduce the three pulses of the wind speed, which is believed to be the main feature leading to the windshear. Thus, the high resolution numerical simulation seems to be useful in the short-term forecasting of windshear at the Plateau airport under consideration for this particular case.

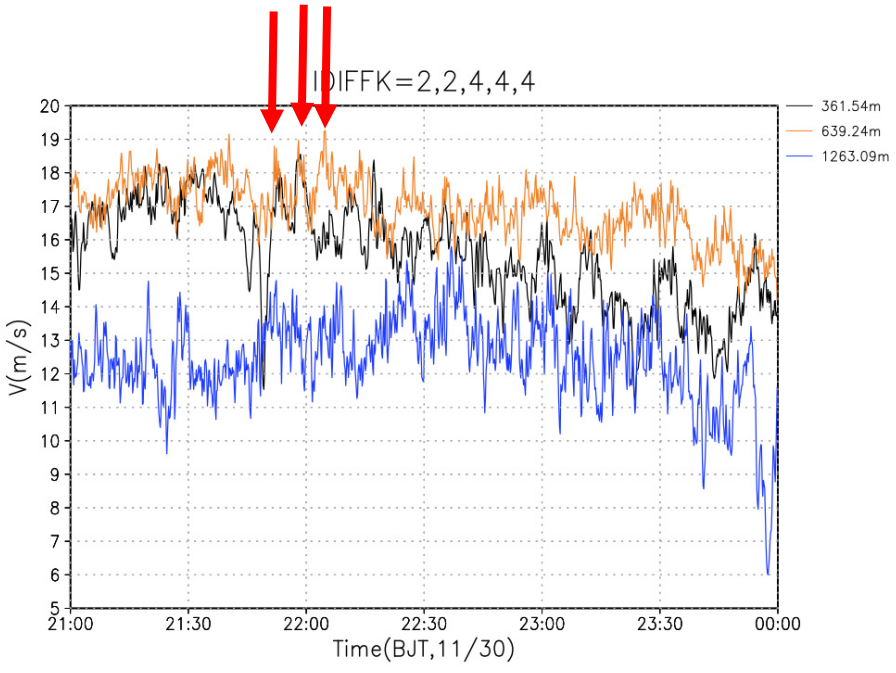

(**a**)

Figure 7. *Cont.*

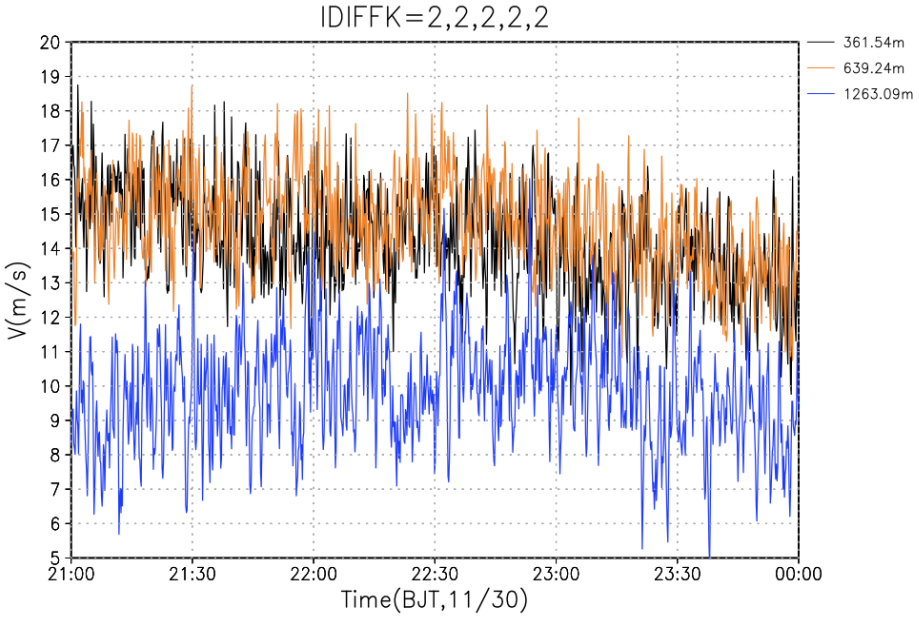

(**b**)

Figure 7. (**a**) is the simulation result of Deardorff scheme. The time series of the simulated wind speed at and around the jet cores. The three pulses of the wind speed are highlighted in arrows. (**b**) is the simulation result of the Smagorinsky scheme.

3.2. Using an Alternative Turbulence Scheme

As in Chan et al. (2022) [13], the choice of turbulence parameterization scheme is studied in this paper, namely, the use of Smagorinsky (1963) [16] scheme for all five domains. The wind-EDR plot from this simulation is shown in Figure 5b. There are a number of short-comings in this simulation, namely:

(a) *The jet core is rather* weak, with a maximum wind speed of around 30 knots only;
(b) The intrusion of westerly wind does not follow the actual observations as closely as in the previous simulation;
(c) The EDRs appear to be rather low and do not show up a clear pattern at the interface between the easterly and westerly on 1 December 2017.

Moreover, the time series of the wind speed is shown in Figure 7b. In general, using this parameterization scheme alone, there are more rapid fluctuations in the wind speed (with a larger error statistically in comparison with actual observations, in the order of 2–3 m/s, as described below), and the distinct pulses of the wind speed in the actual observation do not appear in the simulation. By comparing with the actual observations, it is again confirmed that the Deardorff (1980) [17] scheme, at least for the inner domains, would be more useful in reproducing the windshear features at an area of complex terrain.

Despite being developed in the 1980s, the Deardorff (1980) [17] scheme is still considered to produce realistic results compared with other subscale turbulence model (Gibbs and Fedorovich, 2016) [19] and it has been implemented in many numerical weather prediction models. Alternatively, the Smagorinsky (1963) [16] closure scheme may be used (Gibbs and Fedorovich, 2016) [19]. It is rather common because it is simple to implement and has high numerical stability. However, as pointed out in a number of studies (e.g., Krishnamurthy et al., 2010) [11], the Smagorinsky scheme has only dissipative terms and it may tend to amplify the kinetic energy dissipation. This is consistent with the current results, namely, comparing Figure 5a,b; the latter generally has higher values over height and time, though the maximum value of EDR in Figure 5a is slightly larger. Moreover, both dissipative and productive terms of turbulence are present in the Deardorff (1980) [17] scheme and it may be more realistic in simulating the coherent structures, which take the form of a number of pulses in the easterly wind in the present case (indicated by red arrows

in Figure 3b). This is consistent with the simulation results (Figure 7a versus Figure 7b). The mathematical formulation of the two subgrid scale turbulence closure schemes could be found in the above-mentioned references as well as the documentation of the RAMS model.

To analyze the performance of the two sets of simulations, a comparison between the simulated results and the actual observations is conducted using statistical analysis. The period under consideration covers from 12 UTC to 16 UTC. The heights covered include from 100 m above ground level to 1900 m above ground level. For wind speed, the Deardorff scheme gives a mean absolute error of 1.79 m/s, whereas the Smagorinsky scheme gives 2.44 m/s. For wind direction, the former gives a mean absolute error of 15.3°, whereas the latter gives 17.9°. For EDR, the former gives a mean absolute error of 0.000845 m^2s^{-3}, and the simulated values are positively correlated with the actual observations with a correlation coefficient squared of around 0.16; the latter gives a mean absolute error of 0.00132 m^2s^{-3}, and the simulated values are negatively correlated with the actual observations with a correlation coefficient squared of −0.38. As such, the Deardorff scheme is much better than the Smagorinsky scheme based on the error statistics.

3.3. Mechanical of the Easterly Jet

The simulation results provide the basis to understand the occurrence of low-level jets as shown in the LIDAR's velocity data. For that purpose, the time–height cross section of the simulated horizontal wind and vertical wind at the location of the LIDAR is shown in Figure 8a. It could be seen that, at the times of the occurrence of the pulses of the stronger easterly wind between around 22:00 and 22:30 local time, the simulation result gives quite significant downward velocity. As such, the pulses might be related to the downward transfer of horizontal momentum from heights as high as 1000 m to 1200 m above ground.

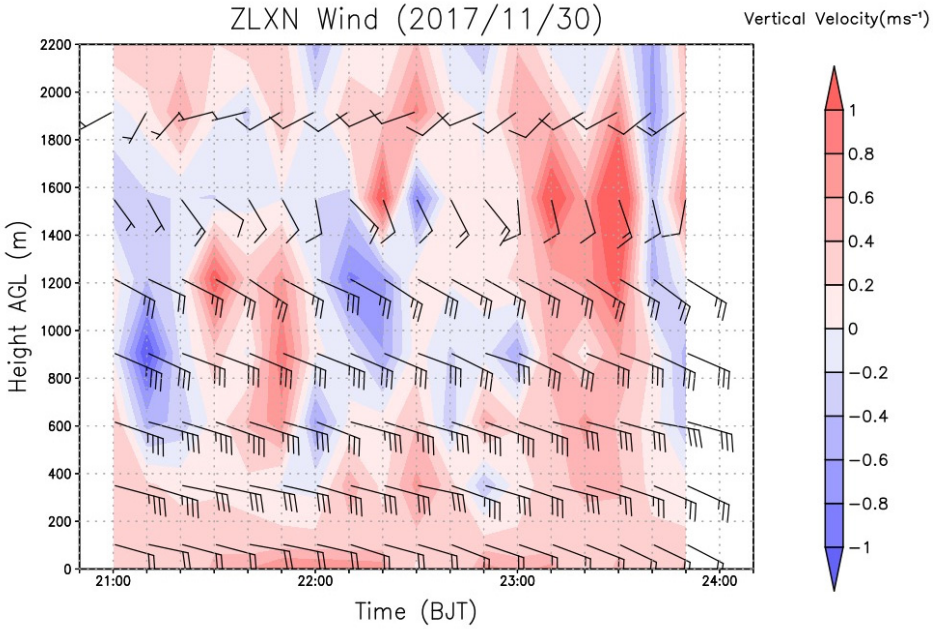

(**a**)

Figure 8. *Cont.*

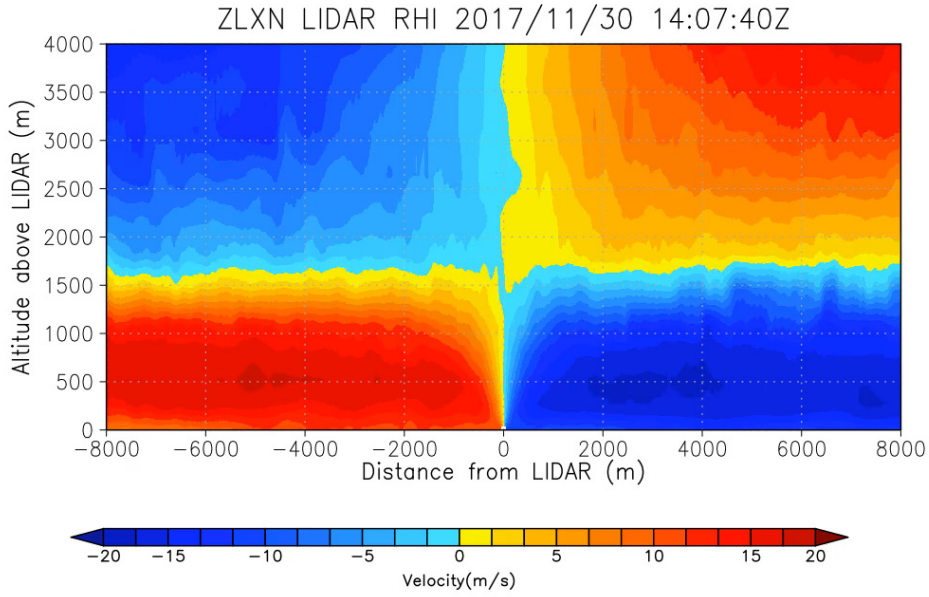

(**b**)

Figure 8. The time–height cross section of the simulated horizontal wind and vertical wind at the location of the LIDAR (**a**) and the simulated range-height indicator image of Doppler velocity of the LIDAR (**b**).

At the same time, the horizontal distribution of wind is also inspected. The LIDAR at the airport has also been configured to perform range-height indicator (RHI) scans, but such Doppler velocity images are not available. Nonetheless, simulated RHI images could be obtained from the simulation data, and a sample is shown in Figure 8b. At the height of the easterly pulses, there are, in fact, streaks of strong horizontal winds (darker blue in the order of 12 m/s for Doppler velocity).

Based on the above results, downward transfer of momentum could be a possible mechanism for the occurrence of the easterly pulses, coupled with the horizontal transfer of the higher wind streaks at the height of the easterly pulses. The simulation results provide a novel view of the mechanism of the easterly pulses for this airport.

3.4. Other Model Setup

The present model setup, similar to one adopted for the Hong Kong International Airport (e.g., [4]), is justified from the satisfactory simulation of terrain-induced windshear features in comparison with actual observations, e.g., from Doppler LIDAR, surface automatic weather stations, and pilot windshear reports. For the complex terrain in Hong Kong, slopes steeper than 30° exist, and the RAMS model version 6.3 is found to perform well with the Deardorff turbulence parameterization scheme.

A possible enhancement to the RAMS simulation is the assimilation of the actual LIDAR data in the running of the model. An experiment with the present model setup has been conducted using the standard data assimilation scheme of RAMS. The vertical wind profiles of the LIDAR and the surface observations are assimilated into the model for an extended period of time, namely, between 12 UTC and 23 UTC on 30 November 2017. The simulation results are compared with the actual LIDAR observations. The same period of data as mentioned above is used for verification purposes. For horizontal wind speed, the RMSE is about 1.96 m/s. For horizontal wind direction, the RMSE is about 15.3°. For EDR, the RMSE is about 0.00083 m^2s^{-3}. All these results are comparable with the model simulation results reported earlier on.

An alternative is to use a numerical model adopted for complex terrain situations. In this regard, the Weather Research and Forecasting model with Immersed Boundary

Method (WRF-IBM, as documented in [20]) is considered because it is explicitly designed to handle complex terrain effects on flow fields at resolutions down to down to 10 m with slopes higher than 30°. All three commonly used parameterization schemes, namely, MYJ, YSU, and MYNN, have been used in WRF-IBM for the simulation. The same period of data as mentioned earlier is used for verification purposes. For horizontal wind speed, the RMSE is in the region of 3.6 to 3.8 m/s. For horizontal wind direction, the RMSE is in the region of 35–37°. For EDR, the RMSE is about 0.00087 m^2s^{-3} to 0.00097 m^2s^{-3}. All these results are comparable or slightly worse than the model simulation results reported earlier.

In future studies, WRF-IBM would be applied to the situation in the Hong Kong International Airport for more extensive comparison with RAMS 6.3—Deardorff parameterization scheme, in order to study the relevant performance of the two models for complex terrain in another place with a more comprehensive actual observation for comparison purposes. The study results would be reported in future papers.

4. Conclusions

This short letter documents a windshear case at an airport at the Plateau and for the first time attempts to simulate the main features of the wind at such an airport using a numerical weather prediction model with high spatial resolution. The actual observations of the windshear are provided by a DWL. The main features of the wind are reasonably well simulated by the numerical model, though there are still a number of limitations such as the maximum wind speed of the jet core, the actual values of EDR, and the timing and height of the intrusion of westerly wind on the following day. Nonetheless, it is shown for the first time that a numerical model with high spatial resolution appears to have the potential for forecasting and fore-warning the occurrence of windshear at an airport at the Plateau. In the previous works (e.g., [6–8]), only isolated terrain near the airport is considered. In the present work, the extensive complex terrain of Qinghai-Tibet Plateau is considered for the first time. The forecasting of windshear using a high-resolution numerical weather prediction model, though with various limitations, could be useful as a tool for an earlier alert of the occurrence of terrain-induced windshear.

More cases of windshear for Plateau airport are being collected. Additional information would be available for more recent cases, such as Quick Access Recorded (QAR) data from the aircraft experiencing windshear, which would provide further insights into the windshear event and the study of the application of numerical modeling in forecasting such wind features. The results will be reported in future papers.

Author Contributions: Methodology, P.W.C.; Software, K.K.L.; Formal analysis, J.Z. and Y.Z.; Investigation, X.S.; Data curation, H.C. All authors have read and agreed to the published version of the manuscript.

Funding: H.C. and X.S. thank the funding support from the World Meteorological Organization's Aviation Research and Development Project Phase 2 (AvRDP2).

Institutional Review Board Statement: Not applicable.

Informed Consent Statement: Not applicable.

Data Availability Statement: The participants of this study did not give written consent for their data to be shared publicly, so due to the sensitive nature of the research, supporting data are not available.

Conflicts of Interest: The authors declare no conflict of interest.

References

1. Boilley, A.; Mahfouf, J.-F. Wind shear over the Nice Côte d'Azur airport: Case studies. *Nat. Hazards Earth Syst. Sci.* **2013**, *13*, 2223–2238. [CrossRef]
2. Hon KK Chan, P.W. Historical analysis (2001–2019) of low-level wind shear at the Hong Kong International Airport. *Meteorol. Appl.* **2022**, *29*, e2063.
3. Shun, C.M.; Chan, P.W. Applications of an Infrared Doppler Lidar in Detection of Wind Shear. *J. Atmos. Ocean. Technol.* **2008**, *25*, 637–655. [CrossRef]

4. Chan, P.W.; Lai, K.K.; Li, Q.S. High-resolution (40 m) simulation of a severe case of low-level windshear at the Hong Kong International Airport—Comparison with observations and skills in windshear alerting. *Meteorol. Appl.* **2021**, *28*, e2020. [CrossRef]
5. Lin, C.; Zhang, K.; Chen, X.; Liang, S.; Wu, J.; Zhang, W. Overview of Low-Level Wind Shear Characteristics over Chinese Mainland. *Atmosphere* **2021**, *12*, 628. [CrossRef]
6. Politovich, M.K.; Goodrich, R.K.; Morse, C.S.; Yates, A.; Barron, R.; Cohn, S.A. The Juneau Terrain-Induced Turbulence Alert System. *Bull. Am. Meteor. Soc.* **2011**, *92*, 299–313. [CrossRef]
7. Hon, K. Predicting Low-Level Wind Shear Using 200-m-Resolution NWP at the Hong Kong International Airport. *J. Appl. Meteor. Climatol.* **2020**, *59*, 193–206. [CrossRef]
8. Chen, F.; Peng, H.; Chan, P.W.; Huang, Y.; Hon, K.K. Identification and analysis of terrain-induced low-level windshear at Hong Kong International Airport based on WRF–LES combining method. *Meteorol. Atmos. Phys.* **2022**, *134*, 1–17. [CrossRef]
9. Ito, J.; Niino, H.; Yoshino, K. Large eddy simulation on horizontal convective rolls that caused an aircraft accident during its landing at Narita Airport. *Geophys. Res. Lett.* **2020**, *47*, e2020GL086999. [CrossRef]
10. Shimoyama, K.; Nakanomyo, H.; Obayashi, S. Airport terrain-induced turbulence simulations integrated with weather prediction data. *Trans. Jpn. Soc. Aero. Space Sci.* **2013**, *56*, 286–292. [CrossRef]
11. Krishnamurthy, R.; Calhoun, R.; Fernando, H. Large-eddy simulation-based retrieval of dissipation from coherent Doppler Lidar data. *Bound. Layer Meteorol.* **2010**, *136*, 45–57. [CrossRef]
12. Schalkwijk, J.; Jonker, H.J.J.; Siebesma, A.P.; Bosveld, F.C. A year-long large-eddy simulation of the weather over Cabauw: An overview. *Mon. Weather Rev.* **2015**, *143*, 828–844. [CrossRef]
13. Chan, P.W.; Lai, K.K.; Li, Q.S. High-resolution simulation of a severe case of low-level windshear at the Hong Kong International Airport: Turbulence intensity and sensitivity to turbulence parameterization scheme. *Atmos. Sci. Lett.* **2022**, *23*, e1090. [CrossRef]
14. Huang, X.; Zheng, J.; Che, Y.; Wang, G.; Ren, T.; Hua, Z.; Tian, W.; Su, Z.; Su, L. Evolution and structure of a dry microburst line observed by multiple remote sensors in a Plateau airport. *Remote Sens.* **2022**, *14*, 3841. [CrossRef]
15. Bouniol, D.; Illingworth, A.; Hogan, R. Deriving turbulent kinetic energy dissipation rate within clouds using ground based radar. *Proc. ERAD* **2004**, 281–285.
16. Smagorinsky, J. General circulation experiments with the primitive equations. Part I, the basic experiment. *Mon. Weather Rev.* **1963**, *91*, 99–164. [CrossRef]
17. Deardorff, J.W. Stratocumulus-capped mixed layers derived from a three-dimensional model. *Bound. Layer Meteorol.* **1980**, *18*, 495–527. [CrossRef]
18. Chow, F.K.; Street, R.L.; Xue, M.; Ferziger, J.H. Explicit Filtering and Reconstruction Turbulence Modeling for Large-Eddy Simulation of Neutral Boundary Layer Flow. *J. Atmos. Sci.* **2005**, *62*, 2058–2077. [CrossRef]
19. Gibbs, J.A.; Fedorovich, E. Sensitivity of turbulence statistics in the lower portion of a numerically simulated stable boundary layer to parameters of the Deardorff subgrid turbulence model. *Q. J. R. Meteorol. Soc.* **2016**, *142*, 2205–2213. [CrossRef]
20. Arthur, R.S.; Lundquist, K.A.; Mirocha, J.D.; Chow, F.K. Topographic Effects on Radiation in the WRF Model with the Immersed Boundary Method: Implementation, Validation, and Application to Complex Terrain. *Mon. Weather. Rev.* **2018**, *146*, 3277–3292. [CrossRef]